JOURNAL OF AIRCRAFT
Vol. 43, No. 6, November–December 2006

CFD/CSD Prediction of Rotor Vibratory Loads in High-Speed Flight

Anubhav Datta,* Jayanarayanan Sitaraman,* Inderjit Chopra,† and James D. Baeder‡
University of Maryland, College Park, Maryland 20742

A computational fluid dynamics (CFD) model is coupled with a computational structural dynamics (CSD) model to improve prediction of helicopter rotor vibratory loads in high-speed flight. The two key problems of articulated rotor aeromechanics in high-speed flight—advancing blade lift phase, and underprediction of pitch link load—are satisfactorily resolved for the UH-60A rotor. The physics of aerodynamics and structural dynamics is first isolated from the coupled aeroelastic problem. The structural and aerodynamic models are validated separately using the UH-60A Airloads Program data. The key improvement provided by CFD over a lifting-line aerodynamic model is explained. The fundamental mechanisms behind rotor vibration at high speed are identified as: 1) large elastic twist deformations and 2) inboard wake interaction. The large twist deformations are driven by transonic pitching moments at the outboard stations. CFD captures 3-dimensional unsteady pitching moments at the outboard stations accurately. CFD/CSD coupling improves elastic twist deformations via accurate pitching moments and captures the vibratory lift harmonics correctly. At the outboard stations (86.5% radius out), the vibratory lift is dominated by elastic twist. At the inboard stations (67.5% and 77.5% radius), a refined wake model is necessary in addition to accurate twist. The peak-to-peak pitch link load and lower harmonic waveform are accurately captured. Discrepancies for higher harmonic torsion loads remain unresolved even with measured airloads. The predicted flap-bending moments show a phase shift of about 10 deg over the entire rotor azimuth. This error stems from 1, 2, and 3/rev lift. The 1/rev lift is unaffected by CFD/CSD coupling. The 2 and 3/rev lift are significantly improved but do not fully resolve the 2 and 3/rev bending moment error.

Introduction

THE objective of this paper is to improve the prediction of rotor vibratory loads by replacing the lifting-line aerodynamic model of a comprehensive rotor analysis with computational fluid dynamics (CFD). The focus is on high-speed level flight of the UH-60A Blackhawk (155 kn, $\mu = 0.368$). The state of the art in helicopter vibration prediction in high-speed flight is far from satisfactory[1] even though both vibratory airloads and structural response show consistent patterns for a large number of helicopters.[2,3] Prediction accuracy of vibratory blade loads is less than 50%. Measurements from the UH-60A Air Loads program[4] open the opportunity to trace back the sources of prediction deficiencies to discrepancies in airload calculation.

Bousman in 1999 (Ref. 5) identified two key discrepancies in articulated rotor aeromechanics: 1) prediction of negative lift phase on the advancing side in high-speed flight and 2) underprediction of pitch link load (by 50%). The error in pitch link load stems from errors in pitching moment predictions. Figure 1 shows state-of-the-art lift and pitching moment predictions from lifting-line comprehensive analyses CAMRAD/JA and 2GCHAS (Ref. 6). The drop in the predicted lift on the advancing side leads the flight-test data by a phase error of around 30 deg.

Reference 7 showed that the lift phase problem is not limited to negative lift near the tip, but stems in general from inaccurate prediction of vibratory lift (3/rev and higher harmonics) all across the blade span. Figure 1 shows the inaccurate prediction of vibratory lift from all comprehensive analyses. Reference 7 further showed that the lift on the advancing blade is dominated by elastic twist. A similar conclusion was drawn earlier by Torok and Berezin[8] using the UH-60A DNW model scale data. Elastic twist is governed by predicted pitching moments. Predicted pitching moments are erroneous, as shown in Fig. 1. Even with accurate pitching moments, Torok and Goodman[9] had shown, predicting elastic twist is a challenging problem. Thus, accurate predictions of lift and pitching moments are coupled to each other via the accuracy of structural response calculation.

Reference 10 decoupled the structural dynamics and aerodynamics of the full-scale UH-60A rotor in high-speed flight. It established that errors in predicted vibratory airloads stem from aerodynamic modeling, not structural dynamic modeling. Given the correct airloads, predicted structural dynamics were satisfactory. On the other hand, given accurate blade deformations, the predicted airloads were unsatisfactory. Only a CFD model (either Navier–Stokes or Euler) predicted the unsteady transonic pitching moments accurately near the tip (86.5% radius outboard). The lifting-line predictions were poor. Lift prediction was good, and similar for both CFD and lifting-line models. The lift phase and vibratory harmonics were accurately captured when the correct elastic twist was prescribed. The goal of the present study is to couple the CFD and CSD (computational structural dynamics) models to predict pitching moments, elastic twist, and vibratory airloads accurately from first principles.

Rotorcraft CFD/CSD coupling can be accomplished in two ways: 1) loose or weak coupling and 2) tight or strong coupling. In loose coupling, airloads and blade deformations are transferred between CFD and CSD once every rotor revolution. In tight coupling, the information exchange occurs at every time step. Obtaining trim solution is significantly easier in loose coupling. Aeroelastic stability analysis, on the other hand, is easier using tight coupling. Altmikus[11] compared the two coupling methods and showed that tight coupling method produces the same airload predictions as the loose coupling method for the same trim state. However, to reach the same trim state, the tight coupling scheme employed needed a 2.5 times greater computational cost compared to loose coupling. Reference 12 has studied tight coupling predictions for the ONERA 7A wind-tunnel rotor.

Loose coupling with a general CSD analysis is an ill-posed problem for rotorcraft. The rotor blade structural frequencies are often

Received 18 July 2005; revision received 23 August 2005; accepted for publication 23 August 2005.

*Assistant Research Scientist, Department of Aerospace Engineering. Member AIAA.
†Alfred Gessow Professor and Director, Alfred Gessow Rotorcraft Center. Lifetime Fellow AIAA.
‡Professor, Alfred Gessow Rotorcraft Center.

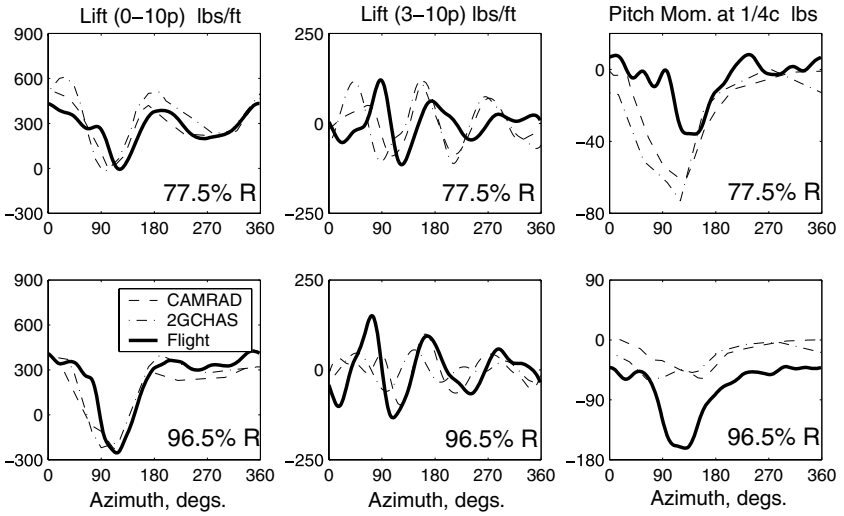

Fig. 1 State-of-the-art airload predictions using lifting-line comprehensive analyses; UH-60A Airloads Program Counter 8534; high-speed level flight at $\mu = 0.368$, $C_W/\sigma = 0.0783$; CAMRAD/JA and 2GCHAS predictions from Ref. 6.

near the excitation harmonics. A general CSD analysis does not contain response-dependent aerodynamic damping. As an example, for a teetering rotor with the first flap frequency at 1/rev and no structural damping, the problem cannot be solved. CFD airloads, when imposed on the structure, would produce resonance at 1/rev. The real airloads contain response-dependent damping terms, and when imposed on the structure produce a zero 1/rev aerodynamic hinge moment. When the response is unknown the aerodynamic hinge moment is not zero. Loose coupling with a comprehensive analysis renders the problem well posed. Here, the aerodynamic damping coefficients from a basic lifting-line calculation are retained. The CFD airloads are imposed as a correction to the lifting-line airloads. The final converged airloads are entirely CFD airloads, independent of the lifting-line aerodynamic model used during convergence. Thus, a simple model can be used as long as it supplies the airload sensitivities to blade deformation.

The loose coupling adopted in this paper follows the delta method proposed by Tung et al.[13] Loose coupling using Euler codes has been performed recently by Altmikus[11] and Servera et al.[14] Loose coupling using Navier–Stokes has been performed by Pahlke.[15] A contemporary study of the UH-60A airloads using Navier–Stokes loose coupling has been carried out by Potsdam et al.[16] The OVERFLOW-D CFD analysis was coupled with CAMRAD comprehensive analysis. In the present study, the TURNS CFD code (transonic unsteady rotor Navier–Stokes, Ref. 17) is coupled with UMARC (University of Maryland advanced rotorcraft code.[7]). The difference between TURNS, as used in the present paper, and OVERFLOW-D is in the implementation of far wake. OVERFLOW-D includes all four blades in the analysis and directly computes the farfield inflow using an overset mesh approach. TURNS, as used here, is a single-blade analysis that obtains the far wake inflow from a free wake model.

The test data used in the present study is from Flight 85 (nominal vehicle weight coefficient, $C_W/\sigma = 0.08$) and Counter 34 (speed 155 kn, with an advance ratio μ of 0.368). All data used and presented in this paper have been corrected for the recent 14-deg azimuthal reference change.[18] The results are presented consistently in the plot database azimuthal reference. The word lift is used interchangeably with normal force throughout this paper.

In the second section, the CSD model is validated using measured airloads. In the third section, a CFD/CSD loose coupling is performed. Within this section, first, the fundamental mechanisms behind rotor vibration at high speed are identified. Then, the motivation behind CFD coupling is explained. The effect of wake interaction on the vibratory airloads is shown. Finally, the coupled airloads and structural loads are validated with flight test data.

Validation of the Computational Structural Dynamics Model

Measured airloads, damper load, and rotor control angles from Flight 8534 are used to validate the structural response of an isolated rotor. Prediction errors originate mainly from structural modeling and from measurement errors in airloads. The rotor blades are modeled as second-order nonlinear isotropic Euler–Bernoulli beams. The coupled flap–lag–torsion equations are based on the second-order accurate (in space) nonlinear beam theory derived in Ref. 19. The formulation is extended to include axial elongation and elastic twist as quasi-coordinates, based on Refs. 20 and 21. The rotor blade is treated as a fully articulated beam with flap and lag hinges coincident at 4.66% span. All blades are identical. Each blade is discretized into 20 finite elements undergoing flap, lag, torsion, and axial degrees of motion.

The tip sweep in the outer 6.9% of the blade span (reaching a maximum of 20 deg at 94.5% span) is modeled in two ways. The baseline model incorporates the tip sweep as a center-of-gravity offset from a straight undeformed elastic axis. The elastic axis of the UH-60A blade is at the local quarter chord line. A refined model incorporates a structurally swept elastic axis. The nonlinear lag damper force is imposed on the structure as a set of concentrated forces and moments acting at 7% of the blade span. The damper-imposed forces and moments vary with azimuth based on the nominal damper geometry. The elastomeric bearing stiffness and damping are modeled as linear springs and dampers in flap, lag, and torsion. The pitch link is modeled as a linear spring–damper system. The first 10 structural modes are used for the present study.

The rotor blade frequencies for soft and stiff pitch links are shown in Figs. 2a and 2b. The root spring stiffness is an equivalent measure of the pitch link stiffness. It is obtained by multiplying the pitch link stiffness with the square of the pitch link arm. The stiffer value of 1090 ft-lb/deg is a more realistic number, as described in Ref. 22. The stiff pitch link increases the first torsion frequency from 3.8/rev to 4.3/rev. The other frequencies remain nominally unchanged. The variation of the first torsion frequency with pitch link stiffness is shown in Fig. 2c. The swept elastic axis model increases the predicted torsion frequency because of increased propeller moment near the tip (Fig. 2c). The predicted frequencies are slightly higher than those predicted in Ref. 22.

The periodic blade response is calculated directly using finite elements in time. The predicted structural loads (mean removed) are shown in Fig. 3. The flap-bending moment (Fig. 3a) shows the right peak to peak and waveform. There is a phase discrepancy of about 5–10 deg around the azimuth. The root chord moment (Fig. 3b) is dominated by the damper force, and shows the same trend as

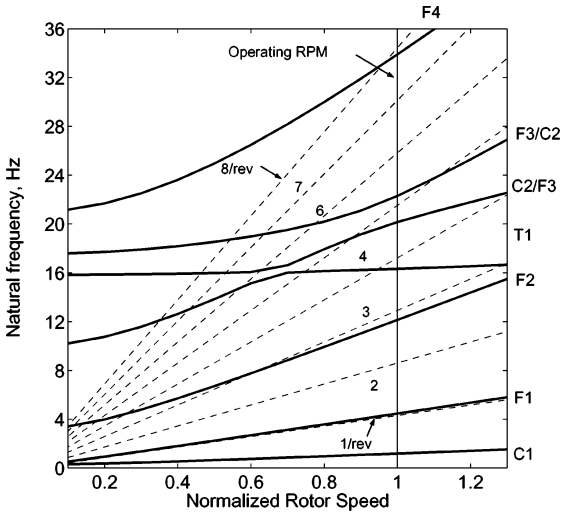

a) Soft pitch-link 363 ft-lb/deg

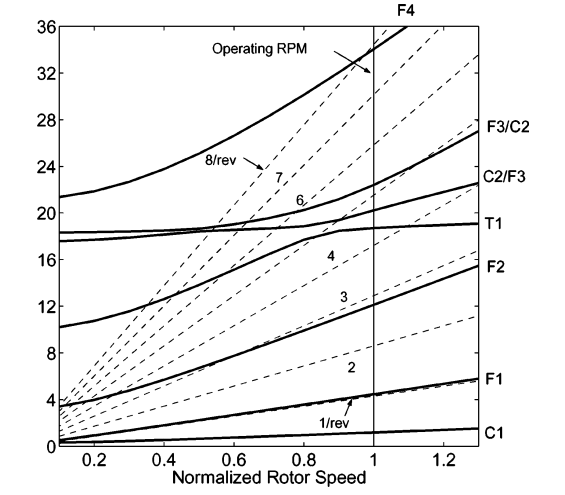

b) Stiff pitch-link 1090 ft-lb/deg

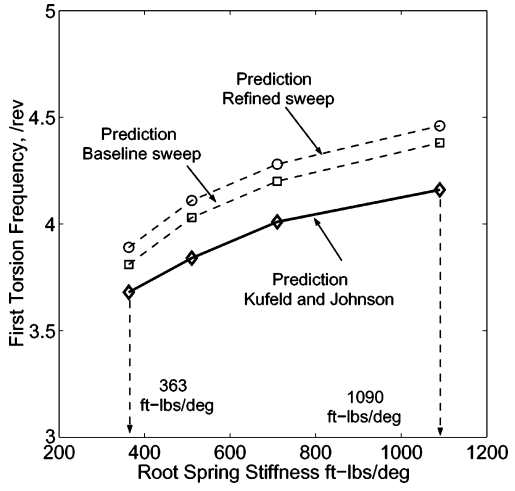

c) Variation of torsion frequency with pitch link stiffness

Fig. 2 UH60A rotor blade frequencies; collective 14.5 deg; effect of root spring stiffness (pitch link stiffness) and structural sweep model.

the test data. The torsion moment (Fig. 3c) is satisfactory in the advancing side but less satisfactory in the retreating side. The integrated effect on the pitch link load is shown in Fig. 3d. The soft pitch link appears to marginally improve predictions on the retreating side (Fig. 3e). The discrepancy stems from inaccurate prediction of 4/rev and higher loads. Neither the soft nor the stiff pitch link resolves this discrepancy. The difference in predictions from the soft and stiff pitch link models is an artifact of the measured airloads problem.

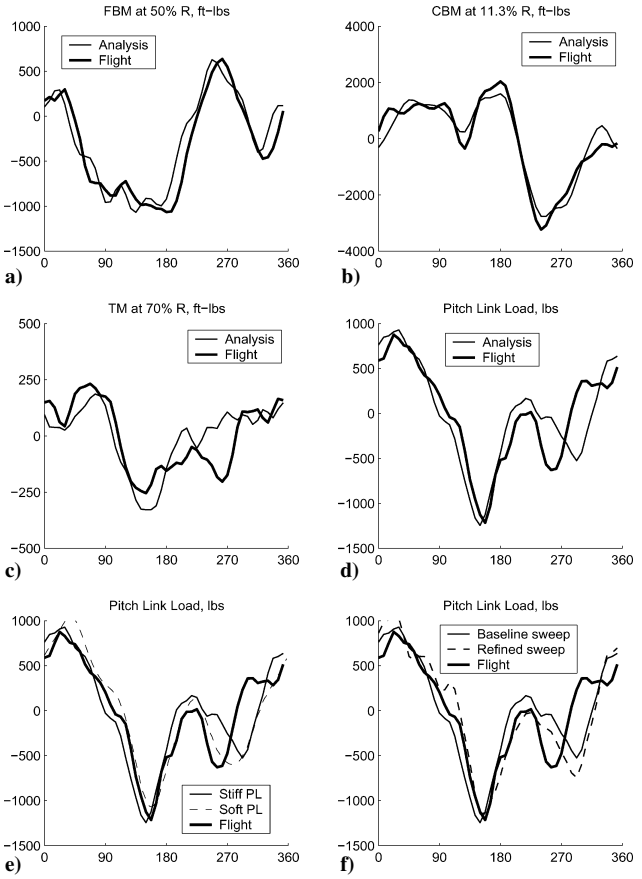

Fig. 3 Predicted and measured structural loads using airloads measured in flight, steadies removed (FBM: flap-bending moment; CBM: chord-bending moment; TM: torsion-bending moment; PL: pitch link; UH-60A Flight 8534, $\mu = 0.368$).

As the first torsion frequency increases from below 4/rev (3.8/rev) to above 4/rev (4.3/rev), the 4/rev response shifts by 180 deg. This is because of zero aerodynamic damping in the system. The shift is not exactly 180 deg, because of a small pitch-bearing damper. The refined sweep model (Fig. 3e) shows similar trends as the baseline model. There is a slight improvement in the advancing side, but the discrepancy in the retreating side remains unresolved.

Computational Fluid Dynamics, Computational Structural Dynamics Loose Coupling

The CFD airloads (normal force, pitching moment, and chord force) are coupled at all radial stations from the root cut out to the tip. The airloads and blade deformations are transferred between CFD and comprehensive analysis at 43 spanwise points. The comprehensive analysis provides the CSD model, a lifting-line model, free wake inflow, and the aircraft trim model. The CSD model is the same as that described above. The stiff pitch link value is used as the baseline. The measured lag damper force is not used. The effect of pitch link stiffness and damper force is shown separately. The lifting-line model provides the airload sensitivities to blade deflection. Three free-wake roll-up models are studied: a tip vortex model, a moving vortex model, and a dual vortex model. The coupling method, the lifting-line model, and the free-wake models are described later.

The trim model is a free-flight propulsive trim for the entire aircraft.[7] The three rotor control angles (collective, longitudinal, and lateral cyclic angles), the aircraft longitudinal and lateral tilts, and the tail rotor collective are calculated based on force and moment balance about the aircraft center of gravity. An alternative trimming method is to target the flight-test measured thrust, hub roll, and pitch moments. The shaft angles are held fixed at measured values. The yaw equilibrium and and the tail rotor collective are neglected. The propulsive trim is adopted here because it does not require measured

thrust and moments as inputs. The airload predictions from both the trim methods were seen to be identical.

The stand-alone UMARC comprehensive analysis is henceforth referred to as the lifting-line analysis. The CFD/CSD coupled analysis is referred to as the CFD analysis.

Computational Fluid Dynamics Model

The CFD computations are performed using an in-house modified version of the TURNS research code (Refs. 23, 24). It is a Reynolds-averaged Navier–Stokes code with a Baldwin–Lomax algebraic turbulence model. TURNS uses a finite difference numerical algorithm that evaluates the inviscid fluxes using an upwind-biased flux-difference scheme (Refs. 25, 26). The van Leer monotone upstream-centered scheme for conservation laws approach is used to obtain second- and third-order accuracy with flux limiters to be total variation diminishing. The lower–upper-symmetric Gauss–Seidel scheme[27] is used as the implicit operator. Though the lower–upper-symmetric Gauss–Seidel implicit operator increases the stability and robustness of the scheme, the use of a spectral radius approximation renders the method only first-order accurate in time. Therefore, second-order backwards differencing in time is used, along with Newton-type subiterations to restore formal second-order time accuracy.

A single block mesh approach is used to make the calculations computationally viable. Complete wake capturing from CFD techniques requires a multiblock or overset mesh-based approach. In this study only one blade of the rotor is modeled and the effects of other blades are included using an induced inflow distribution. The effects of the near-shed wake, near-tip vortex, and bound vortices are captured fairly well in the CFD computations. Hence, only the induced inflow caused by the far-wake tip vortex needs to be included to model the returning wake effects. The induced inflow is computed at each grid point using the Bagai–Leishman free wake model. The induced inflow is incorporated into the flow solution using the field velocity approach, which is a way of modeling unsteady flows via grid movement.[28,29]

The present numerical scheme employs a modified finite-volume method for calculating the grid and time metrics. The modified finite-volume formulation has the advantage that both the space and time metrics can be formed accurately and freestream is captured accurately.[30] The aeroelastic deformations are included into the flow solutions by moving the mesh points to conform to the surface geometry of the deformed blade in a consistent manner. The use of such dynamically deforming mesh geometry mandates the recomputation of space and time metrics at each time step. These quantities are computed in a manner that satisfies the geometric conservation law.[29] The geometric conservation law is used to satisfy the conservative relations of the surfaces and volumes of the control cells in moving meshes.

A body conforming curvilinear meshes that follow a C–H topology is constructed around the UH-60A rotor blade. The C–H grid topology approximates the tip of the blade to a bevel tip. A C–O mesh could provide a better tip definition. Computations performed for the same deflection sets using different grid topologies and mesh refinements are shown in Ref. 17. The coarse mesh uses 133 points in the wraparound direction, of which 99 are on the airfoil surface, 43 points in the normal direction, and 43 points in the spanwise direction. In contrast, the refined mesh used 217 points in the wrap around direction of which 145 are on the airfoil surface, 71 points in the normal direction, and 61 points in the spanwise direction. A C–H mesh is shown in Fig. 4. The spacing of the blade surface in the normal direction is 5×10^{-5} chords for viscous computations and the outer boundaries are 10 chords away from the blade surface.

The details of the grid and time independence studies are described in Ref. 17. The results were found to show good time-step independence. Hence, to facilitate shorter turnaround time for the CFD coupling process, a coarse C–H mesh with azimuthal step 0.5 deg is used for all the computations presented in this paper.

The structural dynamic analysis provides deformations as functions of radius and azimuth of form $[u(r, \psi), v(r, \psi), w(r, \psi), v'(r, \psi), w'(r, \psi), \phi(r, \psi)]^T$, where u, v, w are the linear deformations in axial, lag, and flap directions, v', w' are the radial derivatives of flap and lag degrees, and ϕ is the elastic torsional deformation. The given rotor geometry is dynamically deformed in accordance with these blade motions. At any section, one could define a rotation matrix T_{DU} which is a function of the rotation angles v', w', and ϕ. Then the deformed mesh coordinates in the blade fixed frame are given by the following equation:

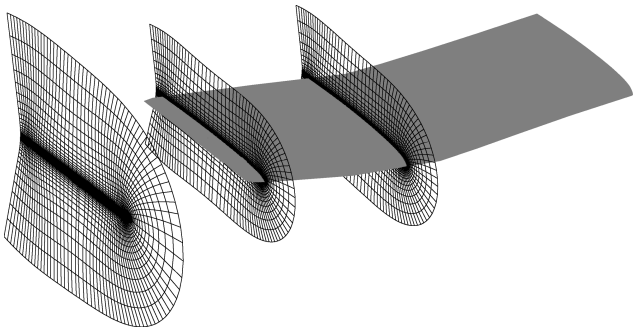

Fig. 4 Near-body *C–H* mesh at the blade tip used for UH-60A airload calculations.

$$\begin{bmatrix} x' \\ y' \\ z' \end{bmatrix} = (T_{DU})^T \begin{bmatrix} x \\ y \\ z \end{bmatrix} + \boldsymbol{x}_{\text{lin}} \tag{1}$$

The vector $\boldsymbol{x}_{\text{lin}}$ represents the linear deflections given by $\{u, v, w\}^T$. Once the deformed mesh is obtained in the blade fixed frame, it is rotated about the z-axis to the appropriate azimuthal location. Cosine decay is applied to both the rotations and linear deflections so that the outer boundary of the mesh remains stationary.

Characteristic boundary conditions are used at the outer boundaries to improve the accuracy of the CFD algorithm. Riemann invariants from the theory of characteristics are satisfied to determine the flow variables and speed of sound at the boundaries. The boundary condition adjusts itself depending on the direction of the flow (into or out of the boundary).

UMARC Lifting-Line Model

The UMARC lifting-line model combines a Weissinger-L near wake,[31] airfoil tables, Bagai–Leishman pseudo-implicit far wake,[32] and the Leishman–Beddoes two-dimensional unsteady model.[33,34] For the unsteady model, the attached-flow formulation is used, because there is no evidence of dynamic stall under this flight condition.[35] The model is semiempirical in nature and has been validated and refined using experimental data from airfoils—NACA 0012, Boeing-Vertol V23010-1.58, and NACA 64A010. Refining the model further for the UH-60A airfoils, SC1095 and SC1094 R8, did not affect airload predictions. Thus, the original Leishman–Beddoes parameters are retained.

The baseline free wake uses a single *tip vortex* model. The vortex is assumed to be fully rolled up, with a strength equal to the maximum bound circulation occurring outboard of 50% span. It is trailed from the tip of the swept elastic axis. In the *moving vortex* model, the vortex is trailed from inboard in the regions of negative lift. The span location from which it is trailed is the zero-bound circulation crossover point. The strength is same as that of the tip vortex model. In the dual vortex model, a negative vortex is trailed from the tip in the regions of negative lift.[36] The possibility of a negative vortex in the tip region was suggested by Ref. 3. The strength of the negative vortex equals the maximum negative circulation attained near the tip. The positive vortex continues trailing from an inboard radial station. Like the moving vortex model, this station is taken at the zero-bound circulation crossover point. The strength of the positive vortex is equal to the sum of the maximum bound circulation occurring outboard of 50% blade radius and the maximum negative circulation occurring near the blade tip. The later is nonzero only in the azimuths of negative lift. All vortices are free. The discretization angle is 5 deg. Two turns of the wake are considered. Increasing

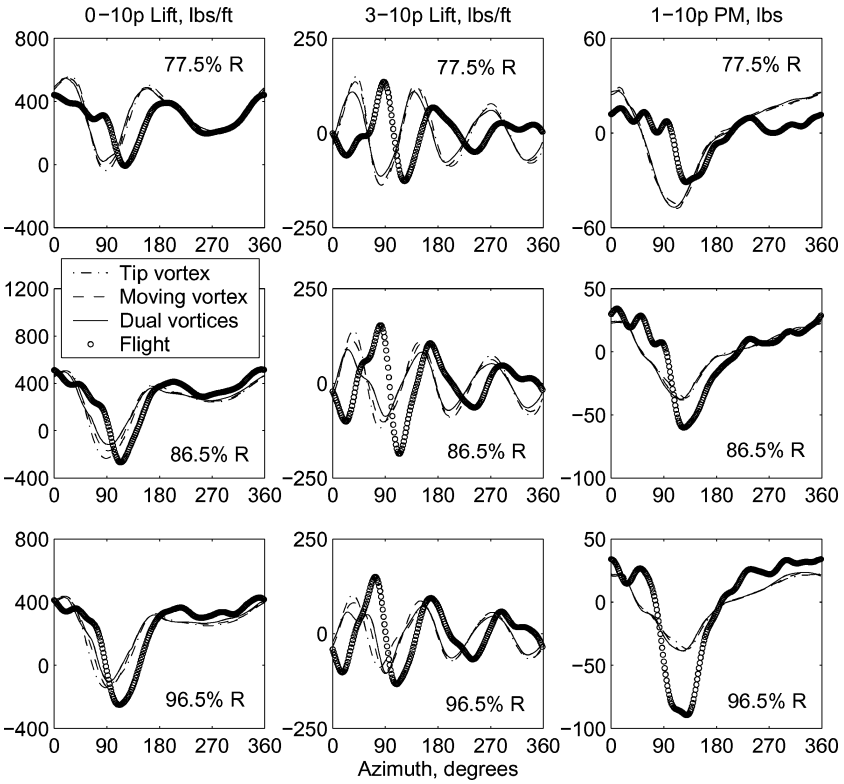

Fig. 5 Predicted airloads from lifting-line comprehensive analysis UMARC (0–10/rev): UH-60A Flight 8534, $\mu = 0.368$.

the discretization angle or the number of turns did not change the airload predictions.

The fuselage aerodynamic properties are incorporated as functions of fuselage tilt. Fuselage dynamics is neglected. The aerodynamic properties are obtained from 1/4-scale wind-tunnel experimental data (from the Ames database). They include the effect of the horizontal tail. The zero-angle fuselage flat plate area is 36.34 ft^2 (Ref. 37). The tail rotor properties and vertical tail cant angle are included. The main rotor has a 3 deg forward shaft tilt angle. The details of the propulsive trim analysis and validation are described in Ref. 7.

The predicted airloads from the lifting-line analysis are compared with test data in Fig. 5. None of the wake models resolve the fundamental deficiency in lift phase or the vibratory lift harmonics in the advancing blade. None of the models accurately predict the unsteady pitching moment variations at the outboard stations. The lifting line predictions, as expected, are similar to those shown in Fig. 1.

Motivation behind Computational Fluid Dynamics Coupling

The motivation behind CFD coupling can be understood by comparing CFD airloads with lifting-line airloads for the same set of blade deformations. The structural model validated before can be used to obtain a set of blade deformations that are close to the actual values in high speed flight. In the absence of measured deformations, this set forms a reasonable basis for comparing the aerodynamic models. The objectives are to identify 1) fundamental differences between lifting-line and CFD predictions, and 2) key mechanisms behind rotor vibration at high speed.

Because of uncertainties in the measured control angles, a calculated set of control angles are used. These are obtained from the lifting-line analysis using measured pitching moments instead of calculated values. This produces a consistent set of elastic twist and rotor control angles. The measured control angles produced a nonphysical negative stall on the advancing side. The deformation set is obtained using a 4% structural damping in the first flap mode. This is required to offset an error in 1/rev aerodynamic flap hinge moment. The error originates from unavoidable errors in measured lift and is discussed in more detail in Ref. 38. Note that the damping is required only while calculating deformations using the measured airloads. For the fully coupled calculations, no artificial damping is used.

Figure 6 shows the predicted lift with the prescribed deformations. The deformations and trim control angles are held fixed for all airload calculations. The rotor is not re-trimmed for the various modeling refinements. Therefore, the 1/rev component of lift is removed for comparison with test data. Compared to Fig. 5, Fig. 6 shows an accurate advancing blade lift phase. Both lifting-line and CFD predictions show the same trends. The improvement in lift stems from accurate 1/rev and 2/rev elastic twist affecting 2/rev and 3/rev blade lift via azimuthal velocity variation. The waveform on the advancing side is accurate near the tip (96.5% R). Inboard (77.5% R), the higher harmonic oscillations on the advancing side are not well captured by elastic twist alone. These oscillations contribute significantly to the vibratory lift phase at the inboard stations. A refined wake model, moving vortex or dual peak, appears necessary in addition to elastic twist. Lifting-line predictions using the dual peak model show marginal improvement compared to the moving vortex model. Therefore, the key phenomenon behind the generation of vibratory lift at the inboard stations appears to be the positive vortex trailed inboard, not the negative vortex trailed from the tip. Figure 7 shows that the radial locations of wake interaction from Blades 4 and 3 on to Blade 1 in the advancing side is significantly altered by the refined wake models. Of the two possible wake interactions, one from Blade 3 and second from Blade 4, the interaction with the wake from Blade 3 appears to play a key role. This is because, from Figs. 7a and 7b, the radial location of wake interaction from Blade 4 on Blade 1 on the advancing side is not significantly altered by the moving vortex model. Only the wake from Blade 3 appears to interact with Blade 1 at a significantly altered radial location.

Accuracy of elastic twist depends on the accuracy of predicted pitching moments. Figure 8 shows that the CFD models provide a fundamentally improved pitching moment prediction near the tip. The waveforms are similar between Euler and Navier–Stokes, showing that the near-wake viscous effects, and hence turbulence modeling, are not dominant factors at this flight condition. The key mechanism appears to be a three-dimensional unsteady transonic effect.[10] The unsteady transonic effect refers to chordwise shock

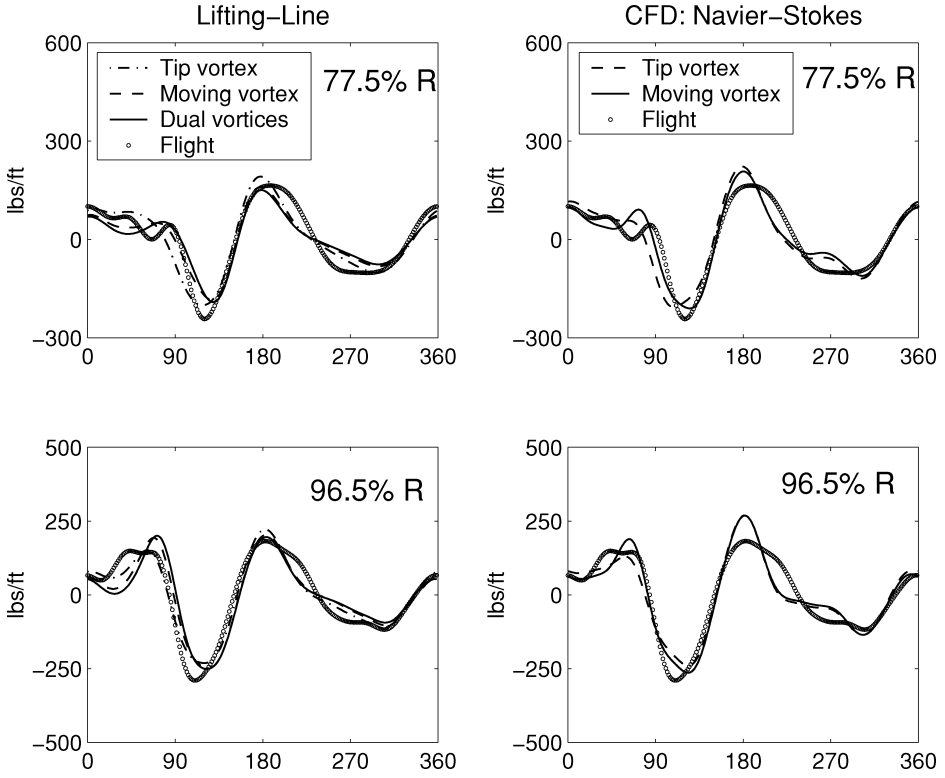

Fig. 6 Predicted and measured lift (2-10/rev) using prescribed blade deformations; UH-60A Flight 8534, $\mu = 0.368$.

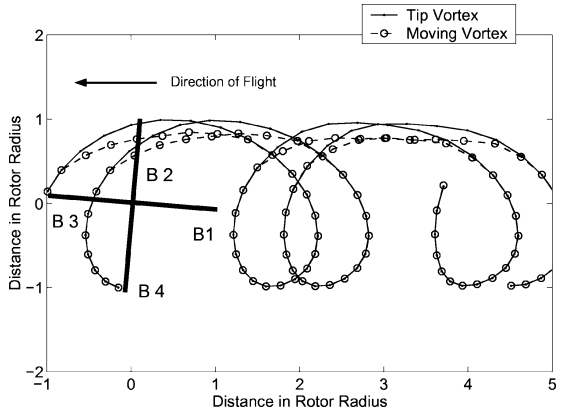

a) Tip and moving vortices

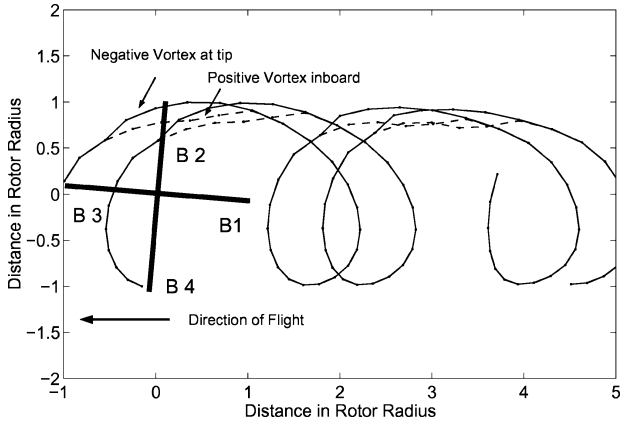

b) Dual peak vortices

Fig. 7 Top view of tip, moving, and dual peak wake geometries using prescribed deformations; UH-60A Flight 8534, $\mu = 0.368$.

movement on the lower surface. The three-dimensional effect refers to a three-dimensional relief near the tip that delays the onset of transonic flow, compared to two-dimensional airfoil properties.

The motivation behind CFD coupling at high-speed flight is therefore to accurately capture the unsteady transonic pitching moments at the outboard stations. Improved pitching moments will provide improved elastic twist. Improved twist, in the presence of a refined wake model, will improve vibratory lift harmonics and the advancing blade lift phase at all radial stations.

Computational Fluid Dynamics, Computational Structural Dynamics Coupling Method

CFD/CSD coupling is performed using the following iterative steps.

1) A lifting-line comprehensive analysis solution is obtained. This provides the baseline blade deformations, trim angles, free wake, and airloads.

2) Using the baseline solution, CFD airloads are calculated. These airloads are different from, and in general improved compared to, the baseline airloads.

3) The differences between the CFD airloads obtained in step 2 and lifting-line airloads are the delta airloads. The lifting-line analysis is now rerun with the delta airloads imposed in addition to the intrinsic lifting-line airloads. The delta airloads are held fixed over the trim iterations. The lifting-line airloads change from one trim iteration to another and provide the airload sensitivities required to trim the rotor. In addition, the lifting-line airloads provide aerodynamic damping, which makes the procedure stable.

4) Steps 2 and 3 are one CFD/CSD coupling iteration. The coupling iterations are performed until the delta airloads converge at every radial and azimuthal station.

The converged airloads are CFD airloads. They are equal to the converged lifting-line airloads plus the converged delta airloads. The converged delta airloads depend on the lifting-line analysis used, but the converged airloads are independent of the lifting-line solution. The baseline CFD/CSD coupling uses the moving vortex wake model. The CFD is run in the Navier–Stokes mode. The effects

Table 1 Lifting-line vs. CFD aircraft trim values

Variable	Flight	LL	CFD
Thrust (lb)	17364	16976	17002
Hub Roll (ft-lb)	6042	6458	5889
Hub Pitch (ft-lb)	−4169	−3866	−3795
Coll. (deg)	13.21	14.5	14.6
Lat. (deg)	5.4	3.2	2.4
Long. (deg)	−9.8	−8.8	−9.3
α (deg)	7.31	8.0	7.9
ϕ (deg)	0.20	−2.3	−2.0
Tail Coll. (deg)	8.7	8.0	6.7

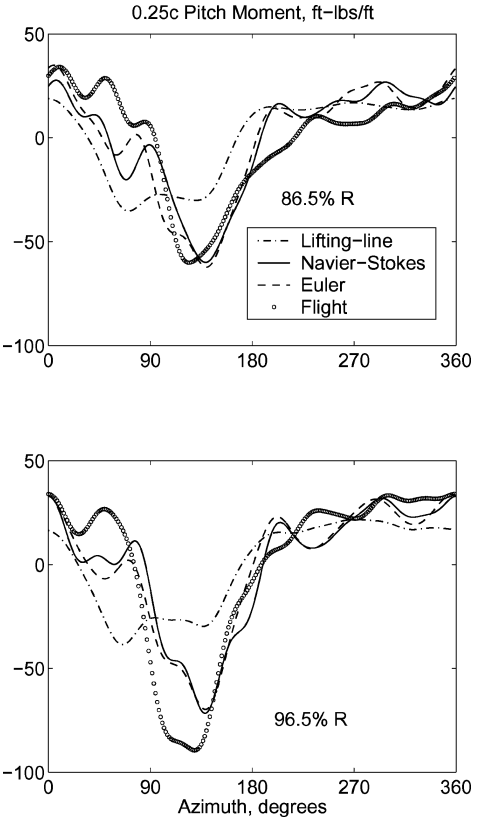

Fig. 8 Predicted quarter-chord pitching moments (1–10/rev) using prescribed blade deformations; UH-60A Flight 8534, $\mu = 0.368$.

of wake (tip vortex versus moving vortex) and near-wake viscosity (Navier–Stokes versus Euler) are shown separately.

The converged trim values are compared with test data in Table 1. The hub roll moment is positive to the left. The hub pitch moment is positive nose up. α is the longitudinal shaft tilt angle, which includes the 3 deg of preshaft tilt. α is positive nose down. The collective angle is defined as the steady pitch angle at the blade root. The results are similar in both cases. In general the lateral trim angle is less satisfactory. The cause of this discrepancy is not clear. However, Ref. 7 showed that the lateral cyclic does not have a significant effect on airload predictions at this flight condition. In addition, as noted earlier, a simpler trim procedure targeting the measured thrust and hub moments produces an identical solution.

The key discrepancy between CFD and lifting-line trim analysis is in the prediction of power. The lifting-line predicted power is accurate (Ref. 7), whereas the CFD shows an underprediction of 20%. The reason for this discrepancy is currently under investigation.

Predicted Airloads

The predicted quarter-chord pitching moments are shown in Fig. 9. Figures 9a and 9b show that the refined wake mainly affects the waveform near the tip, at the junction of the first and second quadrants. Figures 9c and 9d show that Euler and Navier–Stokes

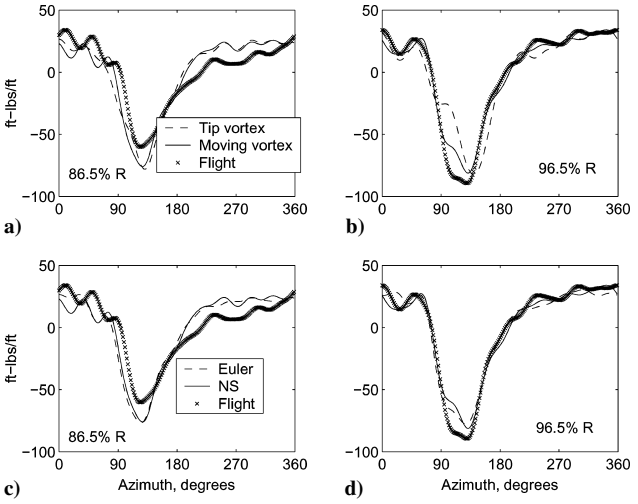

Fig. 9 Predicted quarter-chord pitching moments (1–10/rev) using CFD/CSD coupling; effect of wake and near wall viscosity; UH-60A Flight 8534, $\mu = 0.368$.

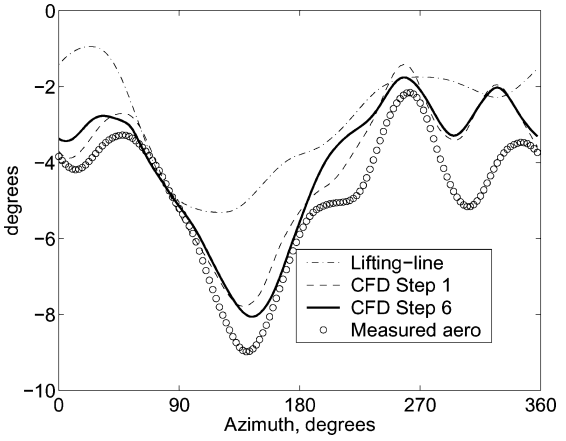

Fig. 10 Evolution of predicted elastic twist over CFD/CSD coupling iterations; UH-60A Flight 8534, $\mu = 0.368$.

coupling capture the peak-to-peak waveform equally well. The improved pitching moment predictions are reflected in the torsion loads later.

Accurate pitching moments generate accurate elastic twist. The evolution of elastic twist over CFD/CSD iterations is shown in Fig. 10. The lifting-line twist corresponds to the lifting-line airloads shown before in Fig. 5. The twist waveform is fundamentally altered from the very first CFD iteration. The 1/rev and 2/rev harmonics are well captured due to the accurate prediction of the transonic pitching moments near the tip (80% R outboard). The converged twist waveform is similar to that obtained earlier using measured airloads. The difference on the retreating side is due to the measured damper force used earlier. The difference in steady offset appears to be due to steady offsets in the test data (96.5% R). Improved elastic twist resolves the phase of the vibratory lift harmonics. The evolution of the vibratory lift harmonics is shown in Fig. 11. Improved vibratory lift harmonics improves the advancing blade lift phase error. Figure 12 shows predicted lift and vibratory harmonics at three radial stations. Predictions using the moving vortex wake model are compared with the tip vortex model.

At the outboard stations (86.5% and 96.5% R), the dominant 3/rev character of the vibratory lift is captured with either wake model. Inboard, the impulsive waveform at the junction of the first and second quadrant appears to be a wake effect. The moving vortex model, as described earlier, shows an improved prediction. The peak-to-peak variation, however, is not accurately captured. The impulse is related to an inboard movement of positive vorticity in the regions of negative lift. For rotors with no negative lift at the tip,

the impulse is not expected to occur. Improving pitching moments alone would then be sufficient to capture the basic pattern of vibratory lift at all radial stations. The SA 349/2 is such a rotor system. A lifting-line analysis for this rotor shows a similar phase error[39] near the tip (0.88% radius). However, the test data do not show an impulse inboard (0.75% radius) like the UH-60A rotor.

Predicted Structural Loads

The predicted torsion loads are shown in Fig. 13. Figures 13a and 13b compare lifting-line predictions to CFD/CSD predictions. Figures 13c and 13d show the effect of pitch link stiffness on CFD/CSD predictions. Figures 13e and 13f show the effect of the measured damper force on CFD/CSD predictions. The effect of CFD/CSD coupling on torsion loads is similar to that on twist deformation seen earlier. The lower harmonics and advancing blade waveform are well captured. The underprediction of peak-to-peak pitch link load is resolved, as shown in Fig. 13b. The higher harmonics (4/rev and higher) are unsatisfactory. The retreating blade error stems from the higher harmonic discrepancy. This is not an aerodynamic discrepancy. It remains, as shown earlier in Fig. 3, even using measured airloads. Figures 13c and 13d show that the pitch link stiffness has a small effect on torsion loads. This is consistent with the conclusion of Ref. 22. The damper force affects the retreating blade waveform. The effect is more pronounced for the soft pitch link, Fig. 13f, compared to the stiff pitch link, Fig. 13e. However, the waveform on the retreating side is still not accurately resolved. The higher harmonic errors remain. This does not appear to be a fundamental deficiency in the structural model, but related to the kinematic boundary conditions at the root end.

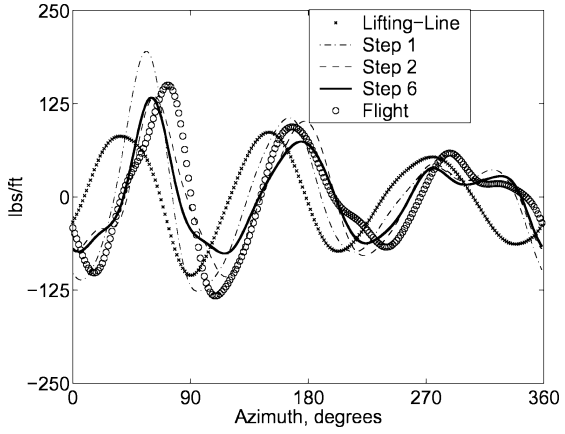

Fig. 11 Evolution of predicted vibratory lift 3–10/rev over CFD/CSD coupling iterations; UH-60A Flight 8534, $\mu = 0.368$.

Figure 14 shows the predicted flap bending moments. The lifting-line and CFD predictions both use the moving vortex model. Both predictions show a shift in phase of about 15–20 deg compared to the test data all over the rotor azimuth. The only improvement obtained using CFD is in the second quadrant. Thus, even though CFD coupling improves lift prediction, predicted flap bending moments do not show a significant improvement in phase. The flap-bending moments are now studied in more detail.

Study of Flap-Bending Moment

CFD flap-bending moments are improved in the second quadrant because of improved inboard lift on the advancing side (55% R–77.5% R). Improved inboard lift on the advancing side stems from the refined wake model in presence of correct elastic twist. Figures 15a and 15b show the effects of wake and twist on lift and flap-bending moments. Consider Fig. 15a. The lifting-line prediction is the same as that shown earlier in Fig. 5. As shown there, it was not significantly affected by the wake models. Tip vortex and moving vortex models produced similar trends. The tip vortex and moving vortex models produce different trends with CFD coupling. This is because CFD coupling generates the correct twist. In the presence of the correct twist, the refined wake improves

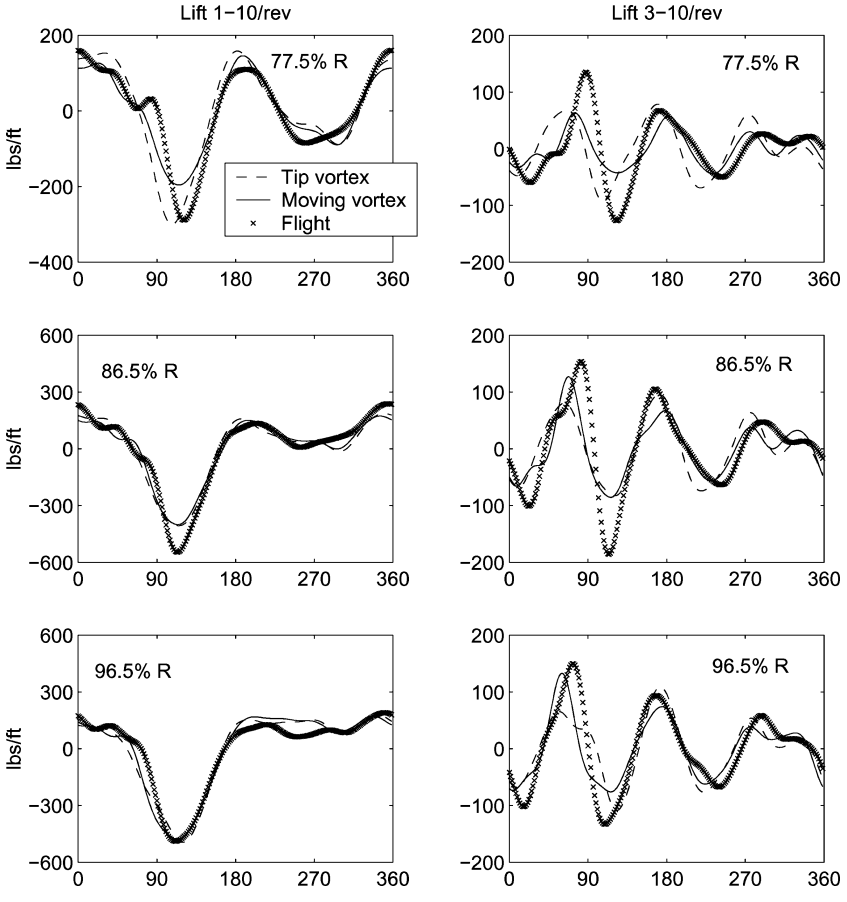

Fig. 12 Predicted lift using CFD/CSD coupling; effect of refined wake model; UH-60A Flight 8534, $\mu = 0.368$.

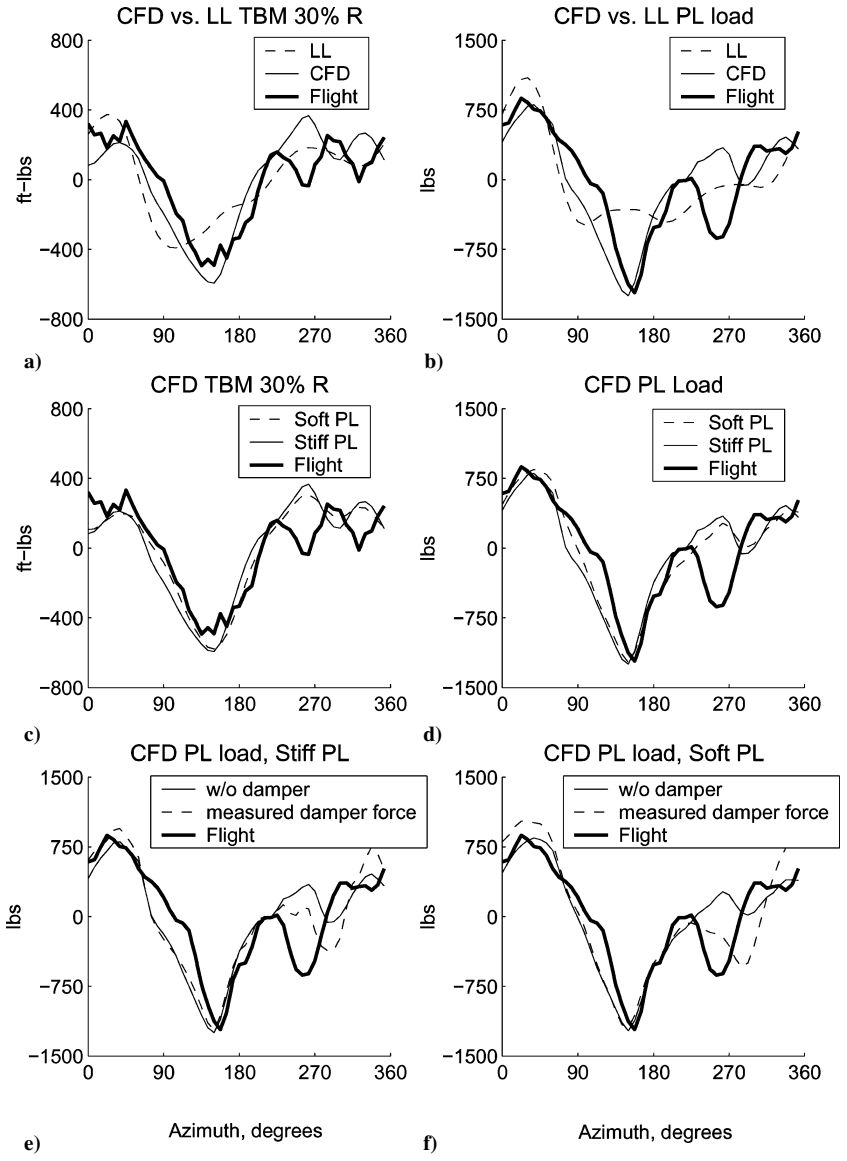

Fig. 13 Predicted torsion loads using CFD/CSD coupling, steadies removed; UH-60A Flight 8534, $\mu = 0.368$.

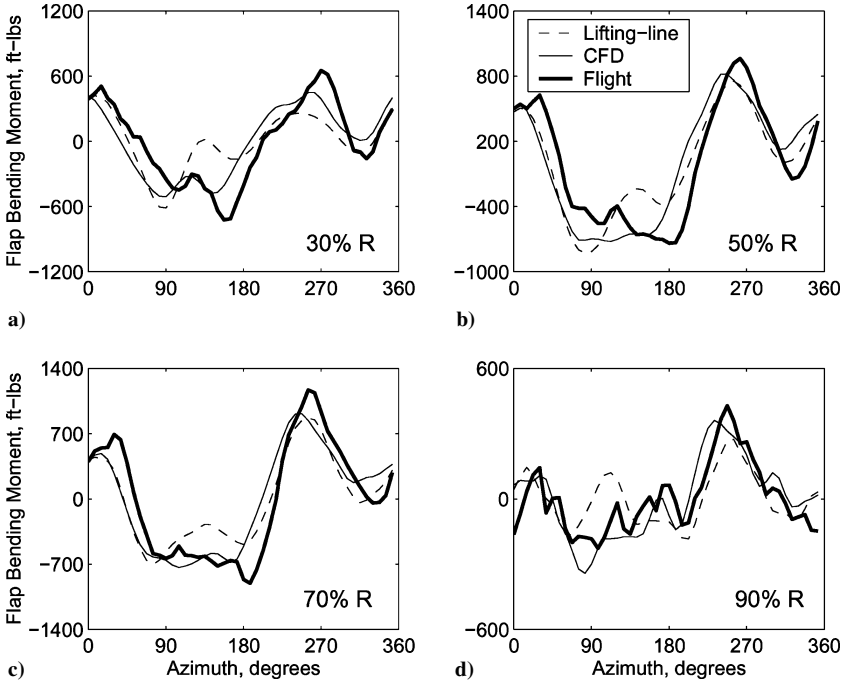

Fig. 14 Predicted flap-bending moments using CFD/CSD coupling, steadies removed; UH-60A Flight 8534, $\mu = 0.368$.

the advancing blade lift waveform inboard. The effect on flap-bending moment is seen in Fig. 15b. The lifting-line moment is similar to CFD with the tip vortex model. CFD with the tip vortex model shows the effect of improved twist alone. CFD with the moving vortex model shows the effect of both improved twist and wake.

The importance of capturing the inboard lift waveform (from 55% R to 77.5% R) can be established by stepwise calculation of flap-bending moments using a combination of flight test and CFD lift. A eight-mode uncoupled flap solution is used for this study, so that the bending moments are generated entirely from blade lift. Figure 16 shows the results from the stepwise calculation. Starting from the CFD results with the tip vortex model, flap bending moments are recalculated by progressively replacing CFD lift with flight-test lift from tip inboard—99% R and 96.5% R to 40% R. The most significant change in the bending moment waveform appears to stem primarily from lift at 67.5% R and 77.5% R. Thus, to summarize, the bending moment waveform is affected more by the inboard lift waveform on the advancing side. Both elastic twist and refined wake are important to capture this effect.

The azimuthal phase discrepancy of 15–20 deg, as shown in Fig. 14, remains unresolved with either wake model. The measured airload results, as in Fig. 3, showed an azimuthal phase error of around 5–10 deg. Thus, between the bending moments obtained using measured airloads and those obtained using CFD/CSD, there is an azimuthal phase shift of around 10 deg. The error progressively increases inboard. Figure 17 shows that the flap-bending moment is dominated by 1–3/rev harmonics. The azimuthal phase of the bending moments therefore depends on the accuracy of the 1–3/rev lift harmonics. The 1–3/rev lift harmonics are significantly improved

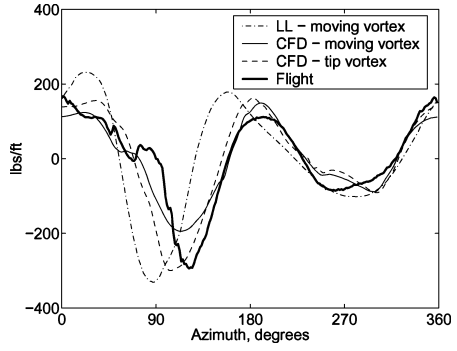

a) Predicted lift improvement from lifting line to CFD, 77.5% R

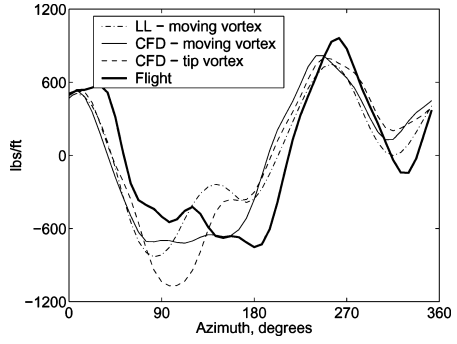

b) Predicted FBM improvement from lifting-line to CFD, 50% R

Fig. 15 Effect of CFD/CSD coupling and refined wake modeling on lift and flap-bending moment prediction; UH-60A Flight 8534, $\mu = 0.368$.

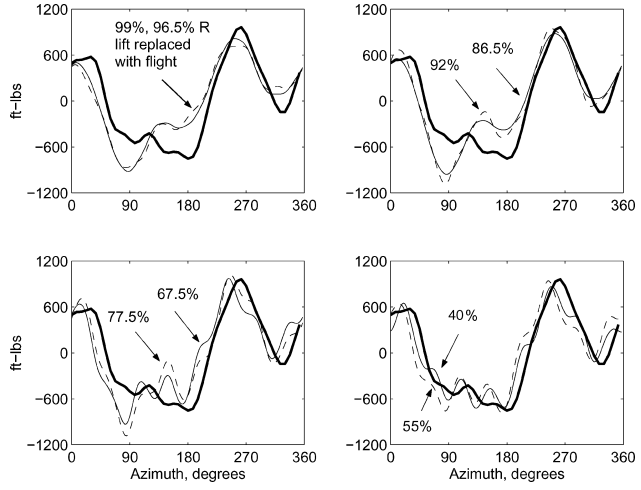

Fig. 16 Investigation of flap-bending moment waveform using measured and predicted lift; 50% R, steadies removed, UH-60A Flight 8534, $\mu = 0.368$.

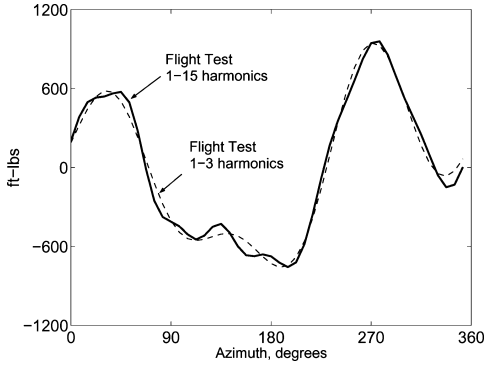

Fig. 17 From 1 to 3 harmonics of measured flap-bending moment at 50% R; UH-60A Flight 8534, $\mu = 0.368$.

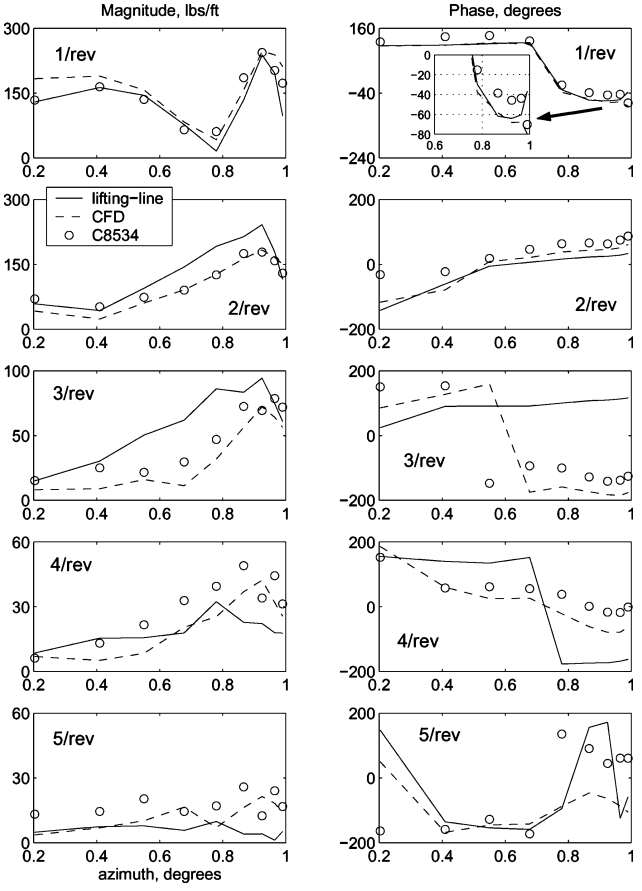

Fig. 18 Contribution of CFD to improving lift harmonics over blade span; CFD-NS with moving vortex, lifting line with moving vortex, UH-60A Flight C8534, $\mu = 0.368$.

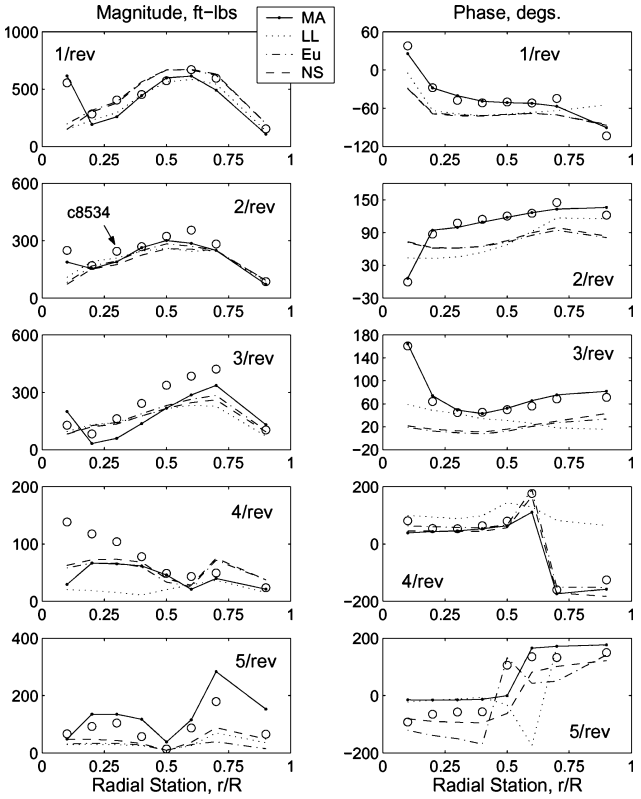

Fig. 19 Measured and predicted flap-bending moment harmonics over blade span; UH-60A Flight C8534, $\mu = 0.368$.

by CFD/CSD coupling. However, this improvement is not enough to fully resolve the bending moment phase.

The problem is studied in Figs. 18 and 19. The fundamental contribution of CFD to lift prediction is summarized in Fig. 18. The phase of 3/rev lift, the dominant vibratory harmonic at high speed, is put in place. In general, the magnitude and phase of all harmonics from 2/rev to 4/rev are improved, accurately, and consistently. This is because the improvement is driven by elastic twist, 1/rev and higher, affecting lift, 2/rev and higher, via the 1/rev azimuthal velocity variation. The 1/rev lift remains unaffected. The phase error in 1/rev lift generates a phase error of 5–10 deg (depending on the radial station) in the 1/rev flap-bending moments. The flap-bending moment harmonics are shown in Fig. 19. Lifting-line predictions are compared with Navier–Stokes and Euler. As expected, both show similar improvements over the lifting-line predictions. Predictions using measured airloads are shown as an upper bound for aerodynamic improvement. As in the case of lift, the phase of all harmonics 2/rev and above is improved by CFD. The spanwise variation of the 2 and 3/rev harmonics, two of the three harmonics that dominate the total flap bending moment waveform, is improved. However, a constant error of approximately 10 deg in azimuthal phase remain all along the span (20 deg phase error in 2/rev, and around 30 deg in 3/rev).

Conclusions

A Reynolds-averaged Navier–Stokes single-blade analysis, TURNS, is loosely coupled to a comprehensive rotor analysis, UMARC, to improve loads prediction for high-speed flight. Measured airloads from the UH-60A Airloads Program are used to validate the structural dynamic model. Once validated, the resultant deformations are used to understand the key benefits of using CFD at high speed. Consistent CFD/CSD coupling is performed to obtain trim, airloads, and structural loads from first principles. Based on this study the following conclusions are drawn.

1) A second-order accurate nonlinear beam theory satisfactorily predicts the structural dynamic loads on an UH-60A rotor in high-speed flight. The 1–3/rev harmonics of torsion are predicted accurately. They are the dominant contributors to advancing blade lift and vibratory harmonics at this flight condition.

2) CFD/CSD coupling captures the three-dimensional unsteady transonic pitching moments near the tip (80% R outboard). Improved pitching moments improve elastic twist predictions. Improved elastic twist predictions improve the vibratory lift phase at all radial stations. The vibratory lift is dominantly 3/rev at the outboard stations. It stems from 2/rev elastic twist. The vibratory lift is more impulsive inboard, and requires both a refined wake and a correct elastic twist for accurate prediction. Without accurate twist, as in the case of lifting-line models, refined wake models alone do not improve lift prediction.

3) CFD/CSD coupling improves prediction of torsion loads. The peak-to-peak and lower harmonics of the pitch–link load are well captured. Error in higher harmonics produces a discrepancy in the retreating blade waveform. In general, the torsion loads are not significantly affected by the pitch link stiffness. However, the effect of the damper force on the pitch link load is affected by the pitch link stiffness.

4) An azimuthal error of 15–20 deg remains unresolved in the flap-bending moment waveform. The measured airloads when imposed on the structural model produce an azimuthal error of 5–10 deg in the bending moments. Thus the remaining discrepancy of around 10 deg stems from predicted airloads.

5) The flap-bending moment waveform is dominated by the 1, 2, and 3/rev harmonics. CFD/CSD coupling does not affect the 1/rev lift. CFD/CSD coupling significantly improves the 2 and 3/rev lift, but not enough to fully resolve the bending moment phase error.

Acknowledgments

This work is a product of the UH-60A Airloads Workshop. The authors gratefully acknowledge the support provided by the National Rotorcraft Technology Center with Yung Yu as technical monitor and all participants of the UH-60A Air loads Workshop organized by U.S.Army/NASA Ames. The authors thank Jim Duh, Alan Egolf (Sikorsky Aircraft Corp.), Robert Ormiston, Mark Potsdam, Wayne Johnson, Hyeonsoo Yeo (Army AFDD and NASA), Bobby Mathew and Ram Janakiram (The Boeing Company) for their collaboration, and significant insights into the problem. This is a revised version of a paper presented at the American Helicopter Society, 60th Annual Forum, Baltimore, MD, June 7–10, 2004.

References

[1]Hansford, R. E., and Vorwald, J., "Dynamics Workshop on Rotor Vibratory Loads Prediction," *Journal of the American Helicopter Society*, Vol. 43, No. 1, Jan. 1998, pp. 76–87.

[2]Bousman, G., "Response of Helicopter Rotors to Vibratory Airloads," *Journal of the American Helicopter Society*, Vol. 35, No. 4, 1990, pp. 53–62.

[3]Hooper, W. E., "Vibratory Airloading of Helicopter Rotors," *Vertica*, Vol. 8, No. 2, 1984, pp. 73–92.

[4]Bousman, G., Kufeld, R. M., Balough, D., Cross, J. L., Studebaker, K. F., and Jennison, C. D., "Flight Testing the UH-60A Airloads Aircraft," *50th Annual Forum of the American Helicopter Society*, Washington, DC, May 1994.

[5]Bousman, G., "Putting the Aero back into Aeroelasticity," *8th Annual ARO Workshop on Aeroelasticity of Rotorcraft Systems*, Pennsylvania State University, University Park, PA, Oct. 1999.

[6]Lim, J. W., and Anastassiades, T., "Correlation of 2GCHAS Analysis with Experimental Data," *Journal of the American Helicopter Society*, Vol. 40, No. 4, 1995, pp. 18–33.

[7]Datta, A., and Chopra, I., "Validation and Understanding of UH-60A Vibratory Loads in Steady Level Flight," *Journal of the American Helicopter Society*, Vol. 49, No. 3, 2004, pp. 271–287.

[8]Torok, M. S., and Berezin, C. R., "Aerodynamic and Wake Methodology Evaluation Using Model UH-60A Experimental Data," *Journal of the American Helicopter Society*, Vol. 39, No. 2, 1994, pp 21–29.

[9]Torok, M. S., and Goodman, R. K., "Analysis of Rotor Blade Dynamics Using Model Scale UH-60A Airloads," *Journal of the American Helicopter Society*, Vol. 39, No. 1, 1994, pp. 63–69.

[10]Datta, A., and Chopra, I., "Validation of Structural and Aerodynamic Modeling Using UH-60A Flight Test Data," *Journal of the American Helicopter Society*, Vol. 51, No. 1, 2006, pp. 43–58.

[11]Altmikus, A. R. M., Wagner, S., Beaumier, P., and Servera, G., "A Comparison: Weak versus Strong Modular Coupling for Trimmed Aeroelastic Rotor Simulation," *58th Annual Forum of the American Helicopter Society*, Montreal, Quebec, June 2002.

[12]Pomin, H., and Wagner, S., "Aeroelastic Analysis of Helicopter Rotor Blades on Deformable Chimera Grids," *Journal of Aircraft*, Vol. 41, No. 3, 2004, pp. 577–584.

[13]Tung, C., Caradonna, F. X., and Johnson, W., "Conservative Full Potential Model for Unsteady Transonic Rotor Flows," *AIAA Journal*, Vol. 25, No. 2, 1987, pp. 193–198.

[14]Servera, G., Beaumier, P., and Costes, M., "A Weak Coupling Method between the Dynamics Code Host and the 3D Unsteady Euler Code Waves," *26th European Rotorcraft Forum*, The Hague, The Netherlands, Sept. 2000.

[15]Pahlke, K., and Van Der Wall, B., "Calculation of Multibladed Rotors in High-Speed Forward Flight with Weak Fluid–Structure-Coupling," *27th European Rotorcraft Forum*, Moscow, Sept. 2001.

[16]Potsdam, M., Yeo, Hyeonsoo, and Johnson, Wayne, "Rotor Airloads Prediction Using Loose Aerodynamic/Structural Coupling," *60th Annual Forum of the American Helicopter Society*, Baltimore, MD, June 7–10 2004.

[17]Sitaraman, J., Baeder, J. D., and Chopra, I., "Validation of UH-60 Rotor Blade Aerodynamic Characteristics Using CFD," *59th Annual Forum of the American Helicopter Society*, Phoenix, AZ, May 2003.

[18]Kufeld, R. M., and Bousman, W. G., "UH-60A Airloads Program Azimuth Reference Correction," *Journal of the American Helicopter Society*, Vol. 50, No. 2, 2005, pp. 211–213.

[19]Hodges, D. H., and Dowell, E. H., "Nonlinear Equations of Motion for the Elastic Bending and Torsion of Twisted Nonuniform Rotor Blades," NASA TN D-7818, Dec. 1974.

[20]Ormiston, R. A., Hodges, D. H., and Peters, D. A., "On the Nonlinear Deformation Geometry of Euler–Bernoulli Beams," NASA Technical Paper 1566, 1980.

[21]Kvaternik, Raymond, G., and Kaza, Krishna, R. V., "Nonlinear Curvature Expressions for Combined Flapwise Bending, Chordwise Bending, Torsion, and Extension of Twisted Rotor Blades," NASA TM X-73, 997, 1976.

[22]Kufeld, R. M., and Johnson, W., "The Effects of Control System Stiffness Models on the Dynamic Stall Behavior of a Helicopter," *54th Annual Forum of the American Helicopter Society*, Washington DC, May 1998.

[23]Srinivasan, G. R., and Baeder, J. D., "TURNS: A Free Wake Euler/Navier–Stokes Numerical Method for Helicopter Rotors," *AIAA Journal*, Vol. 31, No. 5, 1993, pp. 959–962.

[24]Srinivasan, G. R., Baeder, J. D., Obayashi, S., and McCroskey, W. J., "Flowfield of a Lifting Rotor in Hover: A Navier–Stokes Simulation," *AIAA Journal*, Vol. 30, No. 10, 1992, pp. 2371–2378.

[25]Roe, P. L., "Approximate Riemann Solvers, Parametric Vectors, and Difference Schemes," *Journal of Computational Physics*, Vol. 43, No. 3, 1981, pp. 357–372.

[26]Vatsa, V. N., Thomas, J. L., and Wedan, B. W., "Navier–Stokes Computations of Prolate Spheroids at Angle of Attack," AIAA Paper 87-2627, Aug. 1987.

[27]Jameson, A., and Yoon, S., "Lower–Upper Implicit Schemes with Multiple Grids for the Euler Equations," *AIAA Journal*, Vol. 25, No. 7, July 1987, pp. 929–935.

[28]Paramesvaran, V., and Baeder, J. D., "Indicial Aerodynamics in Compressible Flow—Direct Computational Fluid Dynamic Calculations," *Journal of Aircraft*, Vol. 34, No. 1, 1997, pp. 131–133.

[29]Sitaraman, J., Baeder, J. D., and Iyengar, V., "On the Field Velocity Approach and Geometric Conservation Law for Unsteady Flow Simulations," AIAA Paper 2003-3835, June 2003.

[30]Vinokur, M., "An Analysis of Finite-Difference and Finite-Volume Formulations for Conservation Laws," *Journal of Computational Physics*, Vol. 81, No. 2, 1989, pp. 1–52.

[31]Weissinger, J., "The Lift Distribution of Swept-Back Wings," National Advisory Committee for Aeronautics, Technical Memorandum No. 1120, 1942.

[32]Bagai, A., and Leishman, J. G., "The Maryland Free-Wake Analysis—Theory, Implementation and User's Manual," University of Maryland, Department of Aerospace Engineering, Technical Report Prepared for NASA Langley Research Center, Aeroacoustics Branch, Fluid Mechanics and Acoustics Division, Contract 015-2685, Dec. 1995.

[33]Leishman, G. J., "Validation of Approximate Indicial Aerodynamic Functions for Two-Dimensional Subsonic Flow," *Journal of Aircraft*, Vol. 25, No. 10, 1988, pp. 914–922.

[34]Beddoes, T. S., "Practical Computation of Unsteady Lift," *Vertica*, Vol. 8, No. 1, 1984, pp. 55–71.

[35]Coleman, C. P., and Bousman, G., "Aerodynamic Limitations of the UH-60A Rotor," *American Helicopter Society Aeromechanics Specialists Conference*, San Francisco, Jan. 1994.

[36]Johnson, W., "Wake Model for Helicopter Rotors in High Speed Flight," NASA CR 177507, Nov. 1988.

[37]Yeo, H., Bousman, W. G., and Johnson, W., "Performance Analysis of a Utility Helicopter with Standard and Advanced Rotors," *AHS International Technical Specialists Meeting on Aerodynamics, Acoustics, and Test and Evaluation*, San Francisco, Jan. 2002.

[38]Ormiston, R. A., "An Investigation of the Mechanical Airloads Problem for Evaluating Rotor Blade Structural Dynamics Analysis," *AHS 4th Decennial Specialist's Conference on Aeromechanics*, San Francisco, Jan. 2004.

[39]Yeo, H., and Johnson, W., "Assessment of Comprehensive Analysis Calculation of Airloads on Helicopter Rotors," *American Helicopter Society 4th Decennial Specialist's Conference on Aeromechanics*, San Francisco, Jan. 2004.